Critical avalanches and subsampling in map-based neural networks coupled with noisy synapses

M. Girardi-Schappo,[1] O. Kinouchi,[2,3] and M. H. R. Tragtenberg[1,*]

[1]*Departamento de Física, Universidade Federal de Santa Catarina, 88040-900, Florianópolis, Santa Catarina, Brazil*

[2]*Departamento de Física, FFCLRP, Universidade de São Paulo, 14040-900, Ribeirão Preto, São Paulo, Brazil*

[3]*Center for Natural and Artificial Information Processing Systems, Universidade de São Paulo, São Paulo, Brazil*

(Received 23 August 2012; revised manuscript received 29 May 2013; published 27 August 2013)

Many different kinds of noise are experimentally observed in the brain. Among them, we study a model of noisy chemical synapse and obtain critical avalanches for the spatiotemporal activity of the neural network. Neurons and synapses are modeled by dynamical maps. We discuss the relevant neuronal and synaptic properties to achieve the critical state. We verify that networks of functionally excitable neurons with fast synapses present power-law avalanches, due to rebound spiking dynamics. We also discuss the measuring of neuronal avalanches by subsampling our data, shedding light on the experimental search for self-organized criticality in neural networks.

DOI: 10.1103/PhysRevE.88.024701 PACS number(s): 87.18.Sn, 05.65.+b, 05.45.Ra, 87.19.lc

The hypothesis of self-organized critical (SOC) neural networks is based on theoretical considerations made in the 1990's [1–3] and supported by experimental data obtained in the last decade [4–9]. In particular, the observation of neuronal avalanches motivated the search for computational models presenting this phenomenon [10–13]. The key interest in these simulations is to find what are the conditions for the occurrence of power laws in the size and duration distributions of avalanches. Moreover, some authors showed that the critical state may optimize the dynamical (input) range [10,14], the memory and learning processes [11], and the computational power of the brain [5–7]. However, up to now, the computational models rely on very simplified neuron models such as branching processes [8,15–17] or cellular automata [9,10].

Besides these simple approaches, neurons may be modeled by differential equations [18], such as the integrate-and-fire model [19,20], or by discrete time maps [21,22]. Here, we use the extended Kinouchi-Tragtenberg neuron (KTz) map [23,24], which is a discrete time system with behavior similar to the Hindmarsh-Rose model [25]. KTz presents a very rich set of dynamical behaviors (excitability, bursting, cardiaclike spikes, refractoriness, postsynaptic potential summation, etc.) with a minimal set of parameters (see Fig. 1 and Refs. [21,23,24,26]). Appropriately chosen map-based models can sometimes be more efficiently solved than differential equation-based models [22,26]. The main advantage of choosing a model such as KTz is that it provides a good trade-off between dynamical complexity and computational efficiency.

We connect the KTz neurons with a chemical synapse map [23] in order to build a coupled map lattice [27]. The idea of noise in the brain is not new [28,29], but it is frequently modeled by a background external stimulus in the neuron membrane potential [16,30]. In contrast, here we explore the effect of noise in the synaptic coupling, a well known experimental fact [31–35].

We focus our attention in a square lattice of linear size L, even though recent findings point to a brain organized in a complex network [36–38]. Although not realistic, square lattices may provide insights and expected behaviors of this kind of system when going to a more complex topology. For examples of this approach, see Refs. [11,30,39–41].

Concerning the experimental data for neuronal avalanches, we recall that it is generally subsampled, since only a small fraction f of the neurons of the studied brain region is actually recorded. In such a case, the statistical distributions generated by the sampled neurons may not reproduce the distributions of the entire network activity. Thus, we analyze the full and the subsampled data of our distributions of neuronal avalanches with the same algorithm utilized to detect neuronal avalanches experimentally [9,42]. Data subsampling is not always an issue [43].

The model. Each KTz neuron, labeled by an index $i = 1, \ldots, N$, is given by the three-dimensional map

$$\begin{aligned} x_i(t+1) &= \tanh\left[\frac{x_i(t) - K y_i(t) + z_i(t) + v_i(t)}{T}\right], \\ y_i(t+1) &= x_i(t), \\ z_i(t+1) &= (1-\delta) z_i(t) - \lambda\,[x_i(t) - x_R]\,, \end{aligned} \tag{1}$$

where $x_i(t)$ represents the membrane potential of the ith neuron (fast dynamics), $y_i(t)$ is the return variable, $z_i(t)$ is an adaptive variable (e.g., related to slow currents that govern the refractory period and bursting phenomena), and t is the time step (ts). The parameter δ is the inverse recovery time of $z(t)$, K and T are parameters of the fast subsystem that define spiking, resting, and spiking-resting coexistence regimes [21]. The parameters λ and x_R control the slow spiking and bursting dynamics [23]. All the currents received by the neuron, whether synaptic currents or external stimuli, are summed up in $v_i(t) = I_i^{\text{ext}} + \sum_j I_{ij}^{\text{syn}}$.

Chemical synaptic currents are modeled by [23]

$$\begin{aligned} I_{ij}^{\text{syn}}(t+1) &= \left(1 - \frac{1}{\tau_1}\right) I_{ij}^{\text{syn}}(t) + h_{ij}(t), \\ h_{ij}(t+1) &= \left(1 - \frac{1}{\tau_2}\right) h_{ij}(t) + J_{ij}(t)\Theta(x_j(t)), \end{aligned} \tag{2}$$

where $I_{ij}^{\text{syn}}(t)$ is the synaptic current from neuron j (presynaptic) to neuron i (postsynaptic), $h_{ij}(t)$ is an auxiliary variable for creating more complex synapses (e.g., double-exponential functions), τ_1 and τ_2 are time constants for I_{ij}^{syn} and h_{ij},

*marcelotragtenberg@gmail.com

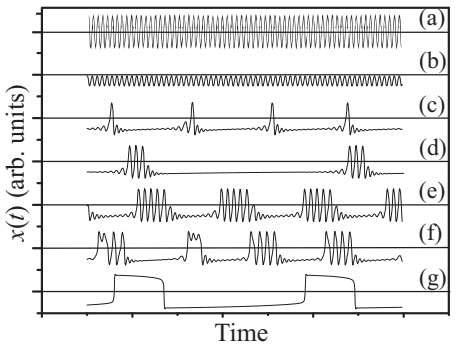

FIG. 1. Examples of KTz behaviors [Eq. (1)] for $K = 0.6$, $I_i(t) = 0$. When not specified, $T = 0.35$ and $\delta = \lambda = 0.001$. (a) Fast spiking ($x_R = -0.2$, $T = 0.45$); (b) subthreshold oscillations ($x_R = -0.5$, $T = 0.45$); (c) slow spiking ($x_R = -0.62$, $\delta = \lambda = 0.003$); (d) slow bursting ($x_R = -0.6$); (e) fast bursting ($x_R = -0.45$); (f) chaotic bursting ($x_R = -0.4$, $T = 0.322$); (g) cardiaclike spiking ($x_R = -0.5$, $T = 0.25$). $x(t)$ is the membrane potential in arbitrary units.

$J_{ij}(t)$ is the coupling parameter ($J_{ii} = 0$), and $\Theta(x)$ is the step (Heaviside) function. Thus, if we start with $I^{\rm syn} = h = 0$, the h variable is activated when the membrane potential is depolarized above zero (which we define as an effective spike duration). This produces an activation of the $I^{\rm syn}$ current, which has a form of a discrete alpha function (for $\tau_1 = \tau_2$) or a discrete double exponential (for $\tau_1 \neq \tau_2$). Notice that the above equations are not used to describe the time evolution of synaptic conductances (as usual) but the evolution of synaptic currents, which is also an acceptable procedure in computational neuroscience [44].

Throughout this Brief Report, we call *inhibitory* the synapses adjusted with parameter $J_{ij}(t) < 0$, although one must bear in mind that, in such a case, the neurons are adjusted in a functionally excitable regime. Thus, the synapses do not inhibit one cell's neighbors. Instead, they may fire rebound spikes [18].

In the homogeneous case, $J_{ij}(t) = J$, any network (whether regular or complex) of excitable neurons with reciprocal synapses and free boundary conditions presents a discontinuous bifurcation transition described by the order parameter M/N (see Fig. 2). Here, M is the number of neurons that fired due to a single delta stimulus and $N = L^2$ is the total number of neurons in the network. Then M/N is the fraction of neurons that participated in the avalanche.

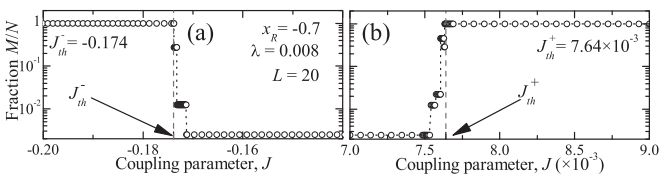

FIG. 2. Fraction of neurons activated by a delta stimulus of intensity $I = 0.1$ in a lattice with $L = 20$ and neurons in regime I and (a) inhibitory synapses or (b) excitatory synapses. $J^-_{\rm th} = -0.174$ ($J^+_{\rm th} = 7.64 \times 10^{-3}$) is the threshold value below (above) which the network is completely activated and it has been determined computationally. It depends only on the neuron parameters.

We show in Fig. 2(a) the case of inhibitory synapses, in which there is a threshold $J = J^-_{\rm th} < 0$ that separates the state in which all the neurons take part in the avalanche ($J < J^-_{\rm th}$) from the state in which only the stimulated neuron, or a few neighbors, responds ($J > J^-_{\rm th}$). A similar transition may occur for excitatory synapses for $J = J^+_{\rm th} > 0$ [Fig. 2(b)].

It is clear from Fig. 2 that the homogeneous model cannot achieve a critical distribution of avalanches, because they are all of size $s = 1$ or N (disregarding the small steps in the phase transition, which are independent of N). Thus, motivated by the synaptic noise present in the brain, we propose the coupling $J_{ij}(t) = J + \epsilon_{ij}(t)$. In the case of inhibitory synapses, $J < 0$ and $\epsilon_{ij}(t) \in [R; 0]$, since $J^-_{\rm th} < 0$. This models a uniform noise, different for every connection $j \to i$ in the network, of maximal amplitude $|R|$, such that $|J + R| > |J^-_{\rm th}|$. Then, the coupling fluctuates near $J^-_{\rm th}$ in an uncorrelated manner.

The noise allows the elements of the network to be either strongly correlated (when $|J_{ij}(t)| > |J^-_{\rm th}|$) or weakly correlated (when $|J_{ij}(t)| < |J^-_{\rm th}|$). These fluctuations spread and dissipate the avalanches. If there is too much noise ($|J + R| \gg |J^-_{\rm th}|$), the avalanches will propagate and dissipate in a completely random fashion; on the other hand, if there is a very small noise ($|J + R| \to |J^-_{\rm th}|$), then the avalanches will soon be dissipated. The balance happens exactly in the critical point (J_c, R_c) in which the avalanches are power-law distributed. This mechanism will be depicted further in Fig. 4.

We can define the probability that $|J_{ij}(t)| > |J^-_{\rm th}|$:

$$p = \frac{J + R - J^-_{\rm th}}{R}. \tag{3}$$

The same holds for excitatory synapses ($J > 0$), where $\epsilon_{ij}(t) \in [0; R]$. The synaptic parameters J and R are, in principle, our control parameters that are adjusted such that there is a nonzero p. For convenience, we utilize p, instead of R, as a control parameter.

Results. We plot the avalanche distributions as cumulative distribution functions. This representation provides a clearer visualization of the data, since it is a continuous function of its variables, it has very reduced noise, its precision does not depend on the size of the bins of the distribution's histogram, and it has a better defined cutoff [45]. Here, s is the amount of spikes in an avalanche and t is the amount of time windows during which the avalanche took place. A given data set with probability distribution function $P(s) = Bs^{-\alpha}$ and cutoff Z (B is constant) corresponds to a cumulative distribution

$$F(s) = A + \frac{B}{\alpha - 1} s^{-\alpha+1}, \tag{4}$$

such that $A = -BZ^{-\alpha+1}/(\alpha - 1)$ [46] and $F(s)$ is the probability of measuring any value greater than s.

All results refer to square lattices of linear size L with free boundary conditions and nearest neighbor couplings. The initial conditions for all neurons are the fixed points (x^*, y^*, z^*) for a given set of parameters. The initial conditions $[I^{\rm syn}_{ij}(0), h_{ij}(0)]$ for the synapses are set to zero.

Some dynamical features of neurons and synapses have revealed themselves to be very important for the occurrence of critical avalanches, especially the size of the refractory period and the synapse's characteristic times. If the synapse takes longer to excite the neighbor than the duration of the

refractory period of the presynaptic neuron, then the wave of activity propagates forward and backward in the network, producing self-sustained activity in the form of spiral waves. This reasoning guided us in choosing the following neuron and synapse sets of parameters.

For each simulation, all neurons and synapses have the same parameters. We examine two different excitable regimes: (I) $x_R = -0.7$, $\lambda = 0.008$—neurons can be excited either by positive and by negative inputs, which generates rebound spikes—and (II) $x_R = -0.9$, $\lambda = 0.1$—which can be excited only by positive inputs, having a bigger refractory period than regime (I). The remaining parameters of the neurons are always $K = 0.6$, $T = 0.35$, and $\delta = 0.001$.

The synapses are fast (time constants $\tau_1 = \tau_2 = 2$ time steps), whereas the spike half duration takes ≈6 time steps [23]). If we use a typical value of 1 ms for the half duration, we can set the time scale (1 time step or 1 ts = 1/6 ms) and get $\tau_1 \approx 0.33$ ms, which is also typical for fast synapses [44]. We studied inhibitory ($J < 0$) and excitatory ($J > 0$) synapses for regime I, and excitatory synapses for regime II.

The network is always stimulated in a randomly chosen site. To separate the time scales, we impose that each stimulus happens only after the end of the previous avalanche. The stimulus takes place during 1 ts (a delta stimulus) with intensity I_{ext} sufficient to produce a spike. We use $I_{\text{ext}} = 0.1$ for regime I and $I_{\text{ext}} = 0.4$ for regime II. The simulation is divided in time windows of 20 ts each. These windows are used to count the spikes in the avalanches, just as in the experimental protocol [9,42].

Avalanche size cumulative distributions $F(s) \sim s^{-\alpha+1}$ for $L = 15, 20$, and 30 are shown in Fig. 3(a), whereas the duration cumulative distributions $F(t) \sim s^{-\tau+1}$ are shown in Fig. 3(b), both for neurons in regime I with excitatory by rebound synapses. Fitting Eq. (4) to the curves in Fig. 3 gives $\alpha = 1.35$, $\tau = 1.50$, and a spatial cutoff $Z_s = L^{\gamma}$, with $\gamma = 2.46 \pm 0.02$. Since the avalanches propagate as fragmented spiral [41,47] waves, we expect $\gamma > 2$, as the same neuron may participate more than once in a given avalanche.

Figure 4(a) shows the existence of a critical region for $-0.100 \leqslant J \leqslant -0.15$, since the distributions for $J = -0.100$ and -0.15 show a cutoff power-law shape [Eq. (4)]. On the other hand, Fig. 4(b) shows that for $J = -0.05$ the small

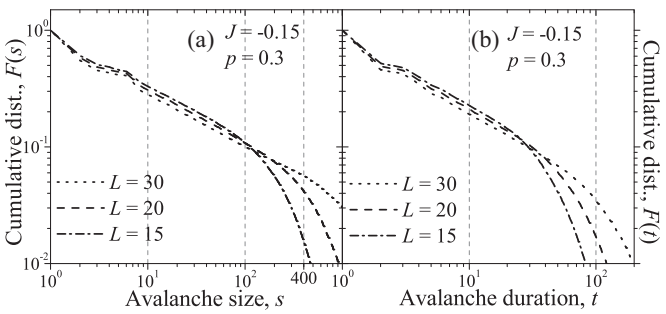

FIG. 3. Simulation data for (a) avalanche size cumulative distributions and (b) avalanche duration cumulative distributions for neurons in regime I, $J = -0.15$, $p = 0.3$, and $L = 15$ (– · –), $L = 20$ (- - -), and $L = 30$ (· · ·). Fitting Eq. (4) to every L gives exponents $\alpha = 1.35$, $\tau = 1.50$, and a spatial cutoff $Z_s = L^{\gamma}$, with $\gamma = 2.46 \pm 0.02$. The fitting is shown in Fig. 6. Remember that $N = L^2$.

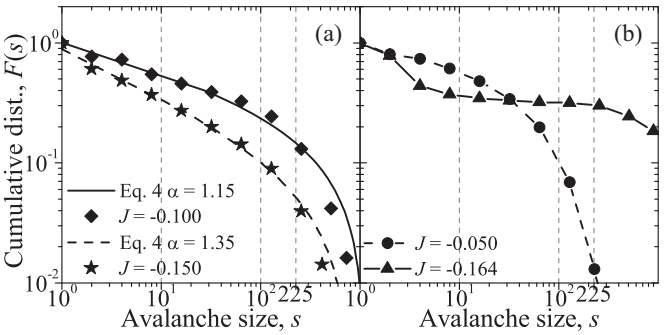

FIG. 4. Avalanche size cumulative distributions for neurons in regime I, $p = 0.3$, $L = 15$ ($N = 225$), and different values of J. (a) Critical regimes for $J = -0.100$ (♦) and $J = -0.150$ (★); lines are Eq. (4) fits of the data, yielding $\alpha = 1.15$ (—) and $\alpha = 1.35$ (– –), respectively. (b) Subcritical regime for $J = -0.050$ (- -●- -) and supercritical regime for $J = -0.164$ (—▲—); the lines are intended only to guide the eyes.

avalanches prevail, characterizing a subcritical regime, while for $J = -0.164$ the large and small avalanches become almost equally likely, which is the signature of a supercritical regime [13]. Notice that, here, by adjusting J with fixed p, we also adjust R [as discussed earlier when Eq. (3) was introduced].

Regarding excitatory synapses ($J > 0$), Fig. 5 show the cumulative distributions of the avalanche sizes for regimes I and II. None of the curves may be fit by Eq. (4), so there is no critical behavior. In fact, these results agree with other authors who have shown that in purely excitatory networks, the cutoff is much smaller than the network size [8].

Reference [9] conjectures that a power-law activity distribution should become a lognormal distribution when the activity measurement is subsampled. If the lognormal distribution [Eq. (5)] is valid only below a cutoff, $s < Z$, then its cumulative distribution function $F(s)$ takes the form of Eq. (6):

$$P(s) = \frac{C}{s\sigma\sqrt{2\pi}} \exp\left\{-\left[\frac{\log(s) - \mu}{\sqrt{2}\sigma}\right]^2\right\}, \tag{5}$$

$$F(s) = \frac{C}{2}\left\{\text{erf}\left[\frac{\log(Z) - \mu}{\sqrt{2}\sigma}\right] - \text{erf}\left[\frac{\log(s) - \mu}{\sqrt{2}\sigma}\right]\right\}, \tag{6}$$

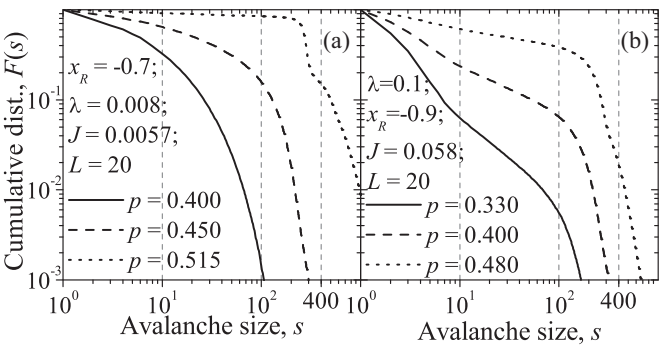

FIG. 5. Avalanche size cumulative distributions for neurons in (a) regime I and (b) regime II for excitatory synapses, $L = 20$ ($N = 400$), and for different excitation probabilities p. Parameters are (a) $J = 0.0057$ and (b) $J = 0.058$.

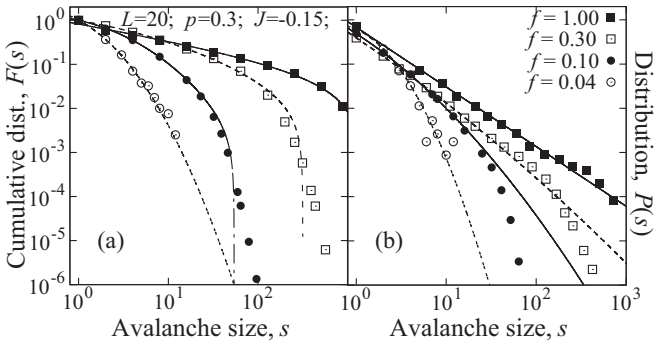

FIG. 6. Simulation data (symbols) and fitted curves (lines) for (a) the cumulative distributions and (b) the distribution functions of the network activity. Neurons are in regime I, with $L = 20$, $p = 0.3$, and $J = -0.15$. $f = 0.04$ (⊙), $f = 0.10$ (●), $f = 0.30$ (⊡), $f = 1.00$ (■). $f = 1.00$ is fitted by (a) Eq. (4) and by (b) $P(s) = Bs^{-1.35}$; the other fractions are fitted by (a) Eq. (6) and (b) Eq. (5).

where C, μ, σ, and Z are fitting constants and $F(s)$ is the probability of measuring any value greater than s.

We simulated the fractions $f = 0.04$, 0.10, 0.30, and 1.00 (the latter is a full sample). The cumulative distribution function is shown in Fig. 6(a), whereas the distribution function is shown in Fig. 6(b). The subsampled data (symbols) in these figures are fitted by Eqs. (5) and (6) (lines), whereas the full sample data is fitted by Eq. (4) [Fig. 6(b)] and its respective distribution [Fig. 6(a)].

As expected, the lognormal distribution fitted well the subsampled $P(s)$ data in Fig. 6(b) [9], mainly for $f = 0.04$. Moreover, the error-function fit in Fig. 6(a) definitely shows that the smaller the fraction f, the more accurate is the fit. The regime of small f is exactly the one we are interested in, because, for current *in vivo* measurements, only a small fraction of the neurons of a mammal's brain, for instance, would be recorded.

Concluding remarks. Since rebound spikes are delayed compared to excitatory spikes, we could only produce power-law avalanches with excitatory by rebound synapses (Figs. 3 and 4). Otherwise, the avalanches are much smaller than the network size (Fig. 5). We also showed that synaptic noise is a way of generating critical avalanches (one would expect it for the same reason that disorder may change a first order phase transition into a second order one [48,49]). Therefore, criticality may be a product of the stochasticity in synaptic interactions, as the noise dissipates the activity just as the inhibitory synapses do in excitatory-inhibitory balanced models [50–52].

Our map-based model presents an out of equilibrium phase transition which we conjecture, following Bonachela *et al.* [39], to pertain to the dynamical percolation universality class. Our next efforts will be to unveil the critical region in the $p \times J$ plane, to study different topologies and heterogeneous networks (mixing excitatory with inhibitory directed synapses). We may also add an extra dynamical rule in the noise amplitude R in order to self-adjust it towards the critical region.

We thank M. Copelli, A. Roque da Silva, D. Arruda, and V. Priesemann for helpful discussions. O.K. acknowledges financial support from the NAP-USP program and from CNAIPS-USP, and M.G.S. was partially supported by CAPES and CNPq.

[1] M. Usher, M. Stemmler, and Z. Olami, Phys. Rev. Lett. **74**, 326 (1995).
[2] D. Stassinopoulos and P. Bak, Phys. Rev. E **51**, 5033 (1995).
[3] A. V. M. Herz and J. J. Hopfield, Phys. Rev. Lett. **75**, 1222 (1995).
[4] D. R. Chialvo, Nat. Phys. **6**, 744 (2010).
[5] G. Werner, Front. Physiol. **1**, 15 (2010).
[6] W. L. Shew and D. Plenz, Neuroscientist **19**, 88 (2013).
[7] J. M. Beggs and N. Timme, Front. Physiol. **3**, 163 (2012).
[8] J. M. Beggs and D. Plenz, J. Neurosci. **23**, 11167 (2003).
[9] T. L. Ribeiro, M. Copelli, F. Caixeta, H. Belchior, D. R. Chialvo, M. A. L. Nicolelis, and S. Ribeiro, PLoS One **5**, e14129 (2010).
[10] O. Kinouchi and M. Copelli, Nat. Phys. **2**, 348 (2006).
[11] L. de Arcangelis, C. Perrone-Capano, and H. J. Herrmann, Phys. Rev. Lett. **96**, 028107 (2006).
[12] L. F. Abbott and R. Rohrkemper, Prog. Brain Res. **165**, 13 (2007).
[13] A. Levina, J. M. Herrmann, and T. Geisel, Nat. Phys. **3**, 857 (2007).
[14] W. L. Shew, H. Yang, T. Petermann, R. Roy, and D. Plenz, J. Neurosci. **29**, 15595 (2009).
[15] C. Haldeman and J. M. Beggs, Phys. Rev. Lett. **94**, 058101 (2005).
[16] D. E. Juanico and C. Monterola, J. Phys. A: Math. Theor. **40**, 9297 (2007).
[17] S. S. Poil, A. van Ooyen, and K. Linkenkaer-Hansen, Human Brain Mapping **29**, 770 (2008).
[18] E. M. Izhikevich, *Dynamical Systems in Neuroscience* (MIT Press, Cambridge, MA, 2007).
[19] A. N. Burkitt, Biol. Cybern. **95**, 1 (2006).
[20] L. Sacerdote and M. T. Giraudo, in *Stochastic Biomathematical Models*, edited by M. Bachar, J. Batzel, and S. Ditlevsen, Lecture Notes in Mathematics (Springer, Berlin, 2013), pp. 99–148.
[21] O. Kinouchi and M. H. R. Tragtenberg, Int. J. Bifurcat. Chaos **6**, 2343 (1996).
[22] B. Ibarz, J. M. Casado, and M. A. F. Sanjuán, Phys. Rep. **501**, 1 (2011).
[23] S. M. Kuva, G. F. Lima, O. Kinouchi, M. H. R. Tragtenberg, and A. C. Roque, Neurocomputing **38–40**, 255 (2001).
[24] M. Copelli, M. H. R. Tragtenberg, and O. Kinouchi, Physica A **342**, 263 (2004).
[25] J. L. Hindmarsh and R. M. Rose, Proc. R. Soc. London, Ser. B **221**, 87 (1984).
[26] M. Girardi-Schappo, M. H. R. Tragtenberg, and O. Kinouchi, J. Neurosci. Methods, doi: 10.1016/j.jneumeth.2013.07.014.
[27] J. R. Chazottes and B. Fernandez, *Dynamics of Coupled Map Lattices and of Related Spatially Extended Systems* (Springer, Berlin, 2005).
[28] A. A. Faisal, L. P. J. Selen, and D. M. Wolpert, Nat. Rev. Neurosci. **9**, 292 (2008).

[29] A. Destexhe and M. Rudolph-Lilith, *Neuronal Noise*, Springer Series in Computational Neuroscience (Springer, Berlin, 2012).
[30] D. R. Chialvo, G. A. Cecchi, and M. O. Magnasco, Phys. Rev. E **61**, 5654 (2000).
[31] B. Katz and R. Miledi, J. Physiol. **192**, 407 (1967).
[32] P. Peretto, *An Introduction to the Modeling of Neural Networks* (Cambridge University Press, Cambridge, UK, 1994).
[33] M. London, A. Schreibman, M. Häusser, M. E. Larkum, and I. Segev, Nat. Neurosci. **5**, 332 (2002).
[34] J. C. López, Nat. Rev. Neurosci. **3**, 332 (2002).
[35] A. O. Komendantov and G. A. Ascoli, J. Neurophysiol. **101**, 1847 (2009).
[36] O. Sporns, G. Tononi, and R. Kotter, PLoS Comput. Biol. **1**, 245 (2005).
[37] O. Sporns, *Networks of the Brain* (MIT Press, Cambridge, MA, 2010).
[38] O. Sporns, *Discovering the Human Connectome* (MIT Press, Cambridge, MA, 2012).
[39] J. A. Bonachela, S. de Franciscis, J. J. Torres, and M. A. Muñoz, J. Stat. Mech. (2010) P02015.
[40] D. Fraiman, P. Balenzuela, J. Foss, and D. R. Chialvo, Phys. Rev. E **79**, 061922 (2009).
[41] X. Wu, J. Ma, F. Li, and Y. Jia, Commun. Nonlinear Sci. Numer. Simul. **18**, 3350 (2013).
[42] V. Priesemann, M. H. J. Munk, and M. Wibral, BMC Neurosci. **10**, 40 (2009).
[43] N. Friedman, S. Ito, B. A. W. Brinkman, M. Shimono, R. E. Lee-DeVille, K. A. Dahmen, J. M. Beggs, and T. C. Butler, Phys. Rev. Lett. **108**, 208102 (2012).
[44] A. Roth and M. C. W. van Rossum, *Modeling Synapses* (MIT Press, Cambridge, MA, 2010).
[45] M. E. J. Newman, Contemp. Phys. **46**, 323 (2005).
[46] V. Priesemann (private communication).
[47] S. J. Schiff, X. Y. Huang, and J. Y. Wu, Phys. Rev. Lett. **98**, 178102 (2007).
[48] K. Hui and A. N. Berker, Phys. Rev. Lett. **62**, 2507 (1989).
[49] C. Van den Broeck, J. M. R. Parrondo, and R. Toral, Phys. Rev. Lett. **73**, 3395 (1994).
[50] B. Haider, A. Duque, A. R. Hasenstaub, and D. A. McCormick, J. Neurosci. **26**, 4535 (2006).
[51] F. Lombardi, H. J. Herrmann, C. Perrone-Capano, D. Plenz, and L. de Arcangelis, Phys. Rev. Lett. **108**, 228703 (2012).
[52] S.-S. Poil, R. Hardstone, H. D. Mansvelder, and K. Linkenkaer-Hansen, J. Neurosci. **32**, 9817 (2012).